Surface processes and kinetics of CO_2 reduction on Pt(100) electrodes of different surface structure in sulfuric acid solutions

Shi-Gang Sun* and Zhi-You Zhou

State Key Laboratory for Physical Chemistry of Solid Surfaces, Department of Chemistry, Institute of Physical Chemistry, Xiamen University, Xiamen 361005, People's Republic of China. E-mail: sgsun@xmu.edu.cn

Received 26th January 2001, Accepted 21st June 2001
First published as an Advance Article on the web 17th July 2001

The reduction of CO_2 on a Pt(100) electrode in CO_2 saturated 0.5 M H_2SO_4 solutions was studied by *in situ* FTIR reflection spectroscopy and a programmed potential step technique. Different surface structures of Pt(100) electrode were prepared by different treatments including fast potential cycling (200 V s^{-1}) for a known time. The Pt(100) surface was characterized by a parameter γ that designates the relative amplitude of the current peak of hydrogen adsorption on (100) sites distributed on the one-dimensional surface domains to that on the two-dimensional surface domains. The *in situ* FTIR spectroscopic results demonstrated that the reduction of CO_2 on the Pt(100) dominated by two-dimensional surface domains produced only bridge-bonded CO (CO_B) species, which give rise to IR absorption near 1840 cm^{-1}. However both bridge- and linear-bonded CO (CO_L, yielding IR absorption at around 2010 cm^{-1}) species are found for CO_2 reduction on the Pt(100) dominated by one–dimensional surface domains. The small intensity of the CO_L and CO_B bands indicates that coverage by reduced CO_2 species (r-CO_2, or CO_L and CO_B species) is low. The cyclic voltammetric (CV) studies confirmed quantitatively the *in situ* FTIRS results, and revealed that the r-CO_2 species adsorb preferentially on (100) sites distributed on the two-dimensional surface domains. The initial rate of CO_2 reduction υ_i, *i.e.*, the rate of CO_2 reduction on a clean Pt(100) surface, has been determined quantitatively from studies using a programmed potential step technique. It has been demonstrated that the maximum values of υ_i (υ_i^m) measured on Pt(100) electrodes with different surface structures all appeared at −0.19 V. From analysis of the relationship between υ_i^m and γ we have determined that the υ_i^m of CO_2 reduction on (100) sites distributed on the two-dimensional surface domains is 0.53×10^{-11} mol cm^{-2} s^{-1} and that on (100) sites distributed on the one-dimensional surface domains is approximately 2.66×10^{-11} mol cm^{-2} s^{-1}. Based on *in situ* FTIRS and electrochemical studies a migration process of the r-CO_2 from the one-dimensional surface domains to the two-dimensional surface domains has been proposed to be involved in CO_2 reduction. The present study has thrown new light on the electrocatalytic activity of different surface structures of a Pt(100) electrode and the surface processes and kinetics of CO_2 reduction.

1. Introduction

Electrochemical reduction of CO_2 is of importance in fundamental studies of electrocatalysis, in environmental applications and in recycling of the carbon resource of the atmosphere. The study of electrochemical reduction of CO_2 has received much attention.[1] Different products of CO_2 reduction, including $H_2C_2O_4$, CO, HCOOH, CH_3OH, HCHO and CH_4, have been determined, depending on the chemical nature of the electrode material and the type of electrolytes.[2–13] Among metal electrodes studied, Pt is unique in that it can reduce CO_2 at low overpotentials.[3,4,6,12,13] Although the electrocatalytic reduction of CO_2 has been investigated intensively, the kinetics and surface processes of CO_2 reduction remain less understood. The use of well-defined single crystal electrodes can provide different models of surface atomic arrangement, and consequently facilitate the study of surface processes of CO_2 reduction at a microscopic level.[3,8–10,14–20] A few groups have studied CO_2 reduction using *in situ* infrared spectroscopy,[2,3,13,16–18] and both linear- and bridge-bonded CO species were found in most cases as the products of CO_2 reduction on Pt single crystal electrodes in acid solutions. In the current paper, emphasis has been put on studies of surface processes and the kinetics of CO_2 reduction on Pt(100) electrodes with different surface structures. From investigations using a programmed potential step technique and *in situ* FTIR reflection spectroscopy, the electrocatalytic activity of different surface structures of a Pt(100) electrode was determined, and the surface processes and the kinetics of CO_2 reduction were clarified.

2. Experimental

The Pt(100) single crystal electrode was prepared in our laboratory according to the procedure described in ref. 21. Before each measurement, the electrode was annealed in a H_2–O_2 flame for a few seconds, cooled in air or in a H_2-stream, then transferred quickly to an electrochemical cell under the protection of a droplet of Millipore water according to Clavilier's method.[22] In order to avoid perturbation of the Pt(100) surface structure by oxygen adsorption at high potentials, the upper limit potential (E_u) in the cyclic voltammetric studies was always below 0.75 V (*vs.* SCE).

A M270 software-controlled 263A potentiostat (EG&G) and an XHD-II potentiostat (Xiamen university) equipped with home-developed software were employed in the electrochemical studies. The latter allowed us to perform a programmed potential treatment on the Pt(100) electrode with fast digital data acquisition.[23] A foil of platinum was applied

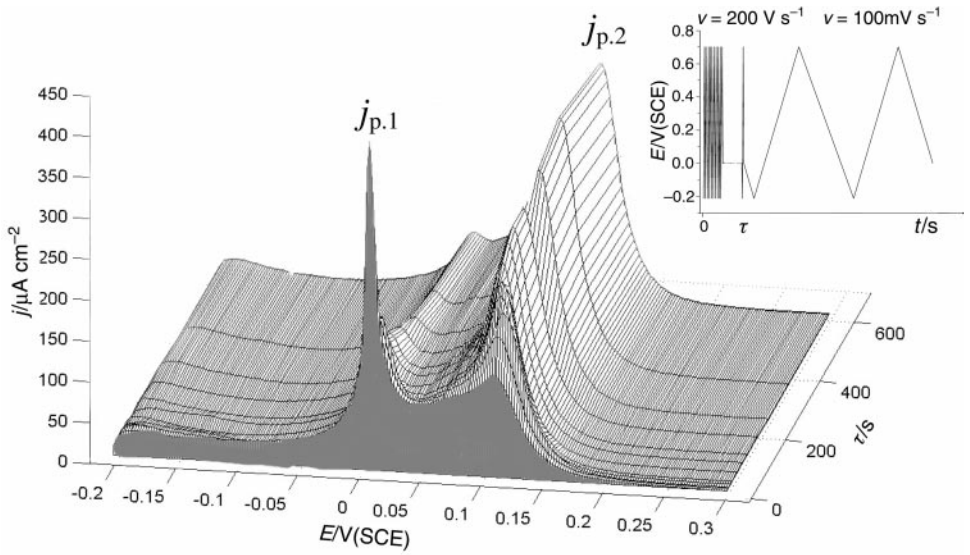

Fig. 1 3-D plot of the variation of the cyclic voltammogram features of a Pt(100) electrode with electrochemical treatment time τ, 0.5 M H_2SO_4 solution, sweep rate 100 mV s^{-1}. The insert illustrates the potential program of electrochemical treatment.

as counter electrode. A saturated calomel electrode (SCE) was employed as reference electrode and potentials in this paper are all referred to the SCE scale. The sulfuric acid solutions were prepared from super-pure H_2SO_4 and Millipore water generated from a Milli-Q Lab system (Nihon Millipore). The solutions were deaerated by bubbling pure N_2 before measurements. The CO_2 gas of high purity (99.995%) was introduced into the solution till saturation for CO_2 reduction. During measurements, a N_2 or a CO_2 gas flow was maintained over the solution to prevent possible interference by contaminants from the atmosphere.

In situ FTIR reflection spectroscopic experiments were carried out on a Nexus 870 FTIR apparatus (Nicolet) equipped with an EverGlo™ IR source and a liquid-nitrogen cooled MCT-A detector. The resulting spectrum is defined as the potential difference spectrum,[24] *i.e.* $\Delta R/R = (R(E_S) - R(E_R))/R(E_R)$, with $R(E_R)$ and $R(E_S)$ the single-beam spectra collected respectively at a reference potential E_R and at a sample potential E_S. For each resulting spectrum 1000 interferograms were scanned at E_R and E_S, and co-added into each single-beam spectrum. The spectral resolution was 8 cm^{-1}.

All experiments were carried out at room temperature, around 22 °C.

3. Results and discussion

3.1 Characterization of Pt(100) surface structures by cyclic voltammetry

In order to study in detail the surface processes and kinetics of CO_2 reduction, it is important to prepare Pt(100) electrodes with different surface structures. Fig. 1 shows a series of j–E curves recorded in 0.5 M H_2SO_4 solution on a Pt(100) electrode that was cooled in air after flame annealing and subjected to a treatment of fast potential cycling (illustrated by the insert to this figure) for different times τ. We can observe two current peaks, $j_{P,1}$ and $j_{P,2}$, at 0.018 and 0.115 V. Following the increase in τ, $j_{P,1}$ decreases, while $j_{P,2}$ increases. It is well known[25–29] that $j_{P,1}$ and $j_{P,2}$ correspond respectively to hydrogen adsorption on (100) sites distributed on one- and two-dimensional surface domains. The variation of $j_{P,1}$ and $j_{P,2}$ with τ indicates that the surface structure of a Pt(100) electrode can be altered continuously by applying a treatment of fast potential cycling.[25,27] Two typical surface structures of the Pt(100) electrode are the Pt(100) cooled in air after flame treatment (denoted as Pt(100)-(1)) and that cooled in a H_2-stream (named Pt(100)-(2)). The voltammograms recorded on these electrodes are illustrated as voltammogram d in Fig. 4 and Fig. 5, see later. We can see that the Pt(100) electrode cooled in a H_2-stream after flame treatment or subjected to a treatment of fast potential cycling will have increased $j_{P,2}$, *i.e.*, the two-dimensional surface domains will be increased. Kolb and co-workers[30] have studied recently the surface structure of a Pt(100) electrode subjected to different treatments using scanning tunneling microscopy and confirmed the existence of one- and two-dimensional surface domains under different experimental conditions. We may define the relative amplitude,

$$\gamma = j_{P,1}/j_{P,2}, \quad (1)$$

as a measure of the relative abundance of one-dimensional surface domains over two-dimensional surface domains on a Pt(100) electrode. γ signifies also the degree of perturbation of a Pt(100) surface. The larger γ, the more one-dimensional surface domains, *i.e.*, step sites and randomly distributed defects, present on a Pt(100) electrode. In other words, a small value of γ would indicate a Pt(100) surface that is dominated by two-dimensional surface domains. The variation of γ *vs.* τ measured from Fig. 1 is plotted in Fig. 2. We can observe that, on increasing τ, γ decreases very quickly at short τ, the rate of decrease then slows and approaches finally the value measured on the Pt(100)-(2) surface. This result demonstrates that we can easily prepare Pt(100) electrodes with different surface structures, and that the two extreme experimental situations are for the Pt(100) cooled respectively in air and in a H_2-

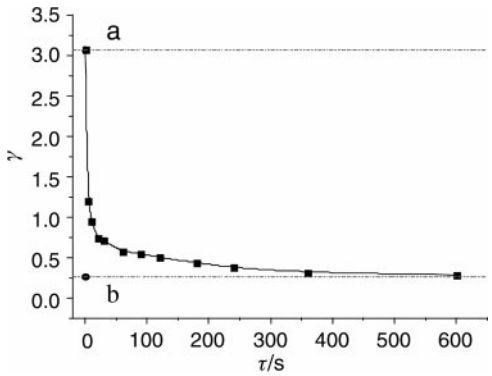

Fig. 2 Variation of γ with τ. The lines a and b are for γ measured on a Pt(100) electrode cooled in air or in a H_2 stream after flame annealing, respectively.

stream after flame annealing. For convenience, we denote as Pt(100)-($\gamma = a$), a Pt(100) electrode that has been subjected to a fast potential cycling treatment.

3.2 Surface processes of CO_2 reduction on Pt(100) electrodes of different surface structure studied by *in situ* FTIRS and cyclic voltammetry

In order to study surface processes and determine the products of CO_2 reduction on Pt(100) electrodes of different surface structure, *in situ* FTIRS experiments were carried out as follows: (1) after characterization of the surface structure of Pt(100) electrode by cyclic voltammetry in 0.1 M H_2SO_4 solution, CO_2 gas of high purity was introduced into the solution; (2) the electrode potential was then held at -0.23 V for 20 min to reduce the CO_2; (3) single-beam spectra $R(E_R)$ and $R(E_S)$ were collected at 0.20 and 0.10 V, respectively. The spectrum a in Fig. 3 was recorded on the Pt(100)-(2) electrode. Only a small bipolar band can be observed, centered at around 1840 cm^{-1} with its positive peak near 1829 cm^{-1} and its negative peak close to 1857 cm^{-1}, this is assigned to IR absorption of bridge-bonded CO species (CO_B) at E_R and E_S.[31–33] A similar result was observed also in 0.1 M $HClO_4$ solution for CO_2 reduction on a well-defined Pt(100) electrode.[18] It is interesting to observe two bipolar bands, near 1840 and 2010 cm^{-1}, in spectrum b recorded on the Pt(100)-(1) electrode. The band centered at around 2010 cm^{-1} with its positive peak near 1995 cm^{-1} and its negative peak close to 2035 cm^{-1} is attributed to IR absorption of linear-bonded CO species (CO_L) at E_R and E_S.[18,31–33] The *in situ* FTIRS results imply that different surface structures of the Pt(100) electrode may exhibit different reactivity and coordination ability for CO_2 reduction. On the Pt(100)-(2) surface only bridge-bonded CO species were formed as the product of CO_2 reduction, however on the Pt(100)-(1) surface both linear- and bridge-bonded CO can be generated. We may infer, from the small intensity of the CO bands in spectra a and b, that the coverage of the r-CO_2 is quite low, though the reduction of CO_2 has been carried out at -0.23 V for 20 min. Korzeniewski *et al.*[34,35] have studied the coverage and potential dependence of CO adsorption at a Pt(335) electrode by using *in situ* FTIR spectroscopy, and demonstrated that at low coverage of CO only linear- and bridge-bonded CO species adsorbed at the (100) step sites of the Pt(335) surface can be determined. The IR features of spectrum b in Fig. 3 confirm that at low coverage of CO the formation of both CO_L and CO_B is favored at the one-dimensional surface domains of Pt(100)-(1) surface. For convenience the term "r-CO_2" is used hereafter to designate the adsorbed product species of CO_2 reduction, *i.e.*, the linear- and bridge-bonded CO species generated in CO_2 reduction.

The spectrum c in Fig. 3 was recorded when CO gas of high purity was bubbled into the solution after recording the spectrum b, and presented IR features of CO co-adsorbed in saturation with the r-CO_2 on the Pt(100)-(1) electrode. Two IR bands, one positive-going band at around 1870 cm^{-1} and a strong bipolar band near 2040 cm^{-1}, can be observed clearly. The former band may be assigned to IR absorption of bridge-bonded CO species mainly at E_R, and the latter band is ascribed to IR absorption of linear-bonded CO species at both E_R and E_S.[36] The significant increase in band intensity and the positive shift of the CO_L band indicate that a relatively quite large amount of CO can adsorb mainly on atop sites at the Pt(100)-(1) surface covered previously with the r-CO_2. The *in situ* FTIRS results imply also that the reduction of CO_2 requires the participation of a few adjacent surface sites, and that the r-CO_2 species may distribute uniformly on the Pt(100) electrode surface.

Cyclic voltammetric studies provided additional experimental evidence on the surface processes of CO_2 reduction. When CO_2 was reduced at -0.20 V for 20 min on the Pt(100)-(1) electrode in 0.5 M H_2SO_4 solution saturated with CO_2, the cyclic voltammograms recorded are shown in Fig. 4. The first voltammogram was recorded between -0.21 and 0.30 V, *i.e.*, in the potential region of hydrogen adsorption. Only one current peak appeared at 0.031 V in the presence of r-CO_2 on the electrode surface. When E_u was increased to 0.70 V the oxidation of the r-CO_2 occurred in a broad current peak centered at 0.520 V of amplitude 275 μA cm^{-2}. The voltammogram recorded immediately after oxidation of the r-CO_2 showed almost complete restoration of the features of the voltammogram for hydrogen adsorption on the Pt(100)-(1) electrode in 0.5 M H_2SO_4 solution, except that $j_{P,1}$ is slightly decreased. This result indicates that the r-CO_2 species have been oxidized completely in the first positive potential scan to 0.70 V. It is interesting to observe that the presence of the r-CO_2 species inhibited mainly hydrogen adsorption on the two-dimensional surface domains. As a consequence the current peak $j_{P,2}$ near 0.115 V has disappeared from the first voltammogram. Moreover, hydrogen adsorption on surface

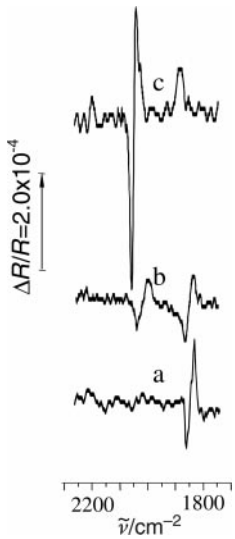

Fig. 3 *In situ* FTIR spectra recorded in CO_2 saturated 0.5 M H_2SO_4 solution. (a) Pt(100) cooled in a H_2 stream, (b) Pt(100) cooled in air, and (c) the solution was bubbled with CO after recording the spectrum b, $E_R = -0.20$ V and $E_S = 0.10$ V. The reduction of CO_2 on the two electrodes was carried out at -0.23 V for 20 min.

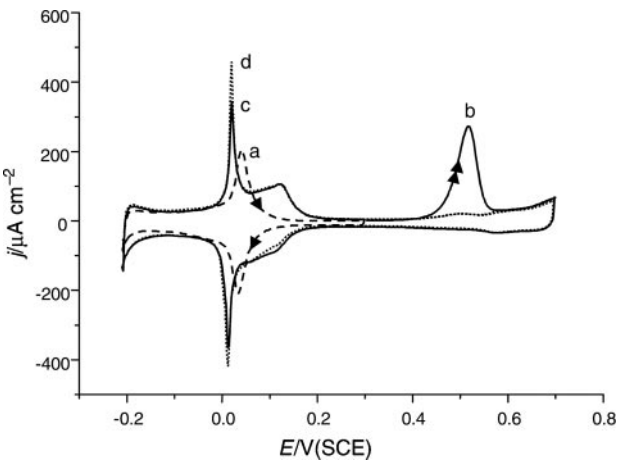

Fig. 4 Cyclic voltammograms of Pt(100) cooled in air after flame annealing in CO_2 saturation 0.5 M H_2SO_4 solution, sweep rate 100 mV s^{-1}. (a) Voltammogram between -0.25 and 0.20 V recorded after a reduction of CO_2 at -0.20 V for 20 min. (b) The oxidation profile of r-CO_2. (c) Voltammogram recorded immediately after the oxidation of r-CO_2. (d) Voltammogram recorded in 0.5 M H_2SO_4 solution.

defects (*i.e.*, the current appearing in the potential range below −0.04 V) is also partially blocked. The current peak $j_{P,1}$ is shifted positively from 0.018 to 0.031 V, and its FWHM is increased from 9.9 to 32.7 mV.

Under the same conditions for CO_2 reduction on the Pt(100)-(2) electrode, *i.e.*, 20 min at −0.20 V in CO_2 saturation 0.5 M H_2SO_4 solution, the voltammograms recorded are displayed in Fig. 5. We can observe, once again, that the presence of the r-CO_2 inhibited mainly the current peak near 0.115 V, *i.e.* the current peak for hydrogen adsorption on the two-dimensional surface domains. The oxidation of the r-CO_2 also yields a broad current peak near 0.50 V of amplitude 237 μA cm^{-2}. The fact that on Pt(100) electrodes of different surface structure the r-CO_2 species inhibit mainly hydrogen adsorption on the two-dimensional surface domains leads us to conclude that the products of CO_2 reduction on Pt(100) electrode are preferentially adsorbed on (100) sites distributed on the two-dimensional surface domains of long range order.

The coverage of the r-CO_2 on the Pt(100) electrode may be calculated from the oxidation charge of the r-CO_2, which can be measured by integration of the CV curves between 0.30 and 0.65 V, *i.e.*, $Q_{ox}^{r\text{-}CO_2} = Q_b - Q_d$, with Q_b and Q_d being the charges integrated respectively from curves b and d. Since the r-CO_2 has been determined as CO_{ad} species by *in situ* FTIRS, the $Q_{ox}^{r\text{-}CO_2}$ should be subjected to a "double-layer" correction according to the method proposed by Gomez *et al.*[37] We have therefore measured the charge displaced (Q_{dis}^{S}) upon saturation adsorption of CO on the Pt(100) electrode,[38] and the charge of CO oxidation (Q_{co}^{S}) of the corresponding saturation coverage. Since the coverage of the r-CO_2 is small, we may presume that the charge displaced upon formation of the r-CO_2 ($Q_{dis}^{r\text{-}CO_2}$) is proportional to $Q_{ox}^{r\text{-}CO_2}$, *i.e.*,

$$Q_{dis}^{r\text{-}CO_2} = \frac{Q_{dis}^{S}}{Q_{CO}^{S}} Q_{OX}^{r\text{-}CO_2}. \quad (2)$$

The coverage of the r-CO_2 after correction for the "double-layer" may be calculated as,

$$\theta_{r\text{-}CO_2} = \frac{N_{r\text{-}CO_2}}{N_{Pt}} = \frac{Q_{OX}^{r\text{-}CO_2} - Q_{dis}^{r\text{-}CO_2}}{2Q_H} = \frac{Q_{OX}^{r\text{-}CO_2}}{2Q_H}\left(1 - \frac{Q_{dis}^{S}}{Q_{CO}^{S}}\right), \quad (3)$$

where $N_{r\text{-}CO_2}$ and N_{Pt} are, respectively, the surface packing densities of the r-CO_2 species and the surface atom on the Pt(100) electrode, and are in direct proportion to ($Q_{OX}^{r\text{-}CO_2} - Q_{dis}^{r\text{-}CO_2}$)/2 and Q_H. A factor 2 is introduced into the formula because the oxidation of each r-CO_2 species will transfer 2 electrons. The values of $\theta_{r\text{-}CO_2}$ that were measured from the CVs of Fig. 4 and Fig. 5 are 0.267 and 0.275, respectively, for CO_2 reduction on the Pt(100)-(1) and the Pt(100)-(2) electrodes at −0.20 V for 20 min. It is worth pointing out that these values are quite small, since we have determined that the saturation coverage of CO adsorption on both the Pt(100)-(1) and the Pt(100)-(2) electrodes is close to 0.745 under the present experimental conditions. If we increase the reduction time the coverage of r-CO_2 may increase slowly. For example, when the reduction of CO_2 was carried out at −0.20 V for 2 h, the $\theta_{r\text{-}CO_2}$ on the Pt(100)-(1) electrode was increased only to 0.356 and that measured on the Pt(100)-(2) to merely 0.389. Since the r-CO_2 are adsorbed species on the Pt(100) surface, the small value of $\theta_{r\text{-}CO_2}$ even after a long time of CO_2 reduction may imply that the reduction of CO_2 requires participation of adjacent surface sites. In considering that the r-CO_2 are distributed uniformly on the Pt(100) surface, as indicated by the *in situ* FTIRS data, the reduction of CO_2 on the Pt(100) electrode will stop when the number of adjacent surface sites available for assisting CO_2 reduction is decreased to a certain extent by increasing the $\theta_{r\text{-}CO_2}$. As a consequence the maximum $\theta_{r\text{-}CO_2}$ is limited to a small value.

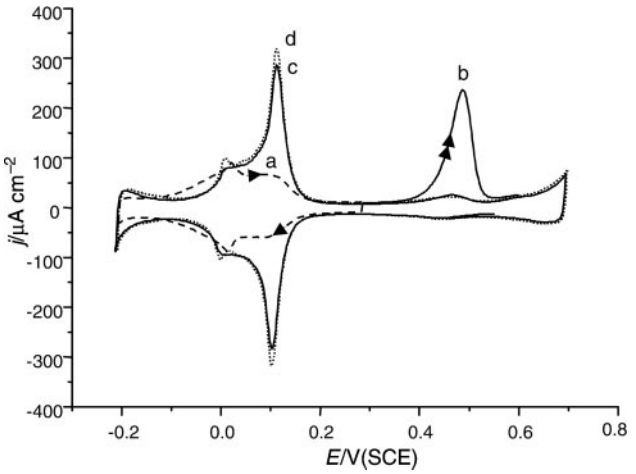

Fig. 5 Cyclic voltammograms of Pt(100) cooled in a H_2 stream after flame annealing in CO_2 saturated 0.5 M H_2SO_4 solution, sweep rate 100 mV s^{-1}. (a) Voltammogram between −0.25 and 0.20 V recorded after a reduction of CO_2 at −0.20 V for 20 min. (b) The oxidation profile of r-CO_2. (c) Voltammogram recorded immediately after the oxidation of r-CO_2. (d) Voltammogram recorded in 0.5 M H_2SO_4 solution.

3.3 Quantitative analysis of the kinetics of CO_2 reduction on Pt(100) electrodes of different surface structure

3.3.1 Determination of the initial rate of CO_2 reduction on a Pt(100) electrode. For accurate measurement of the initial rate of CO_2 reduction (v_i), *i.e.*, the reduction rate of CO_2 on a clean Pt(100) surface, a potential step program was designed and shown in the inset to Fig. 6. This program includes the following steps: (i) The electrode potential is held initially at 0.70 V for 100 ms to oxidize completely any organic adsorbates to get a clean Pt(100) surface. (ii) The potential is then stepped to the reduction potential (E_r) in the potential region of hydrogen adsorption (−0.25–0.2 V). A defined reduction time (t_r) during which the adsorbed products generated from CO_2 reduction were accumulated on Pt(100) surface was used. (iii) It is known from previous cyclic voltammetric studies that, during the reduction of CO_2 at E_r, a certain amount of hydrogen will be co-adsorbed on the Pt(100) surface with the r-CO_2. If the potential is directly stepped to the oxidation potential (E_{ox} = 0.7 V), the oxidation of hydrogen, which forms an important background current, will seriously affect the measurement of the oxidation charge of r-CO_2. To eliminate this effect, the electrode potential is firstly stepped to 0.30 V, a potential in the potential region of double-layer charging, and held for 10 ms to oxidize completely the adsorbed hydrogen. (iv) The potential is finally stepped to the oxidation

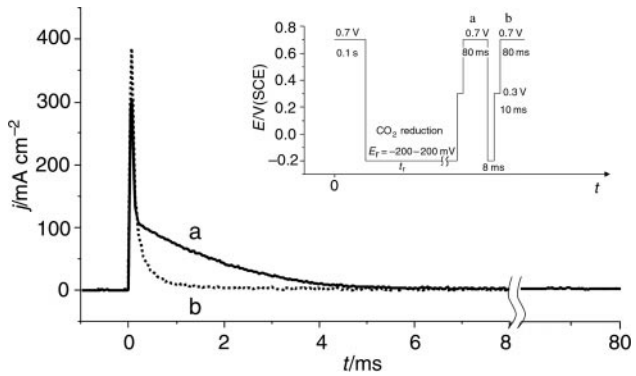

Fig. 6 *j–t* transients of the r-CO_2 oxidation (a) and the background (b) recorded on a Pt(100) electrode cooled in air after flame annealing. The reduction of CO_2 was carried out at E_r = −0.20 V and t_r = 1200 s in CO_2 saturated 0.5 M H_2SO_4 solution. The insert is the potential step program.

potential E_{ox} to oxidize the r-CO_2 species, and the $j(E_r, t_r)$–t transient curve is recorded immediately in a time window of 80 ms. The curve a in Fig. 6 is the $j(E_r, t_r)$–t transient of $E_r = -0.20$ V and $t_r = 20$ min. (v) In order to eliminate interference from other background current, such as the oxygen adsorption, the oxidation of possible impurities in solution at E_{ox}, a background $j(E_r, t_r)$–t transient of $t_r = 8$ ms is recorded immediately, Fig. 6b. The oxidation charge of the r-CO_2 ($Q_{ox}^{r\text{-}CO_2}$) after the "double-layer" correction can be evaluated by integration of the difference of the two curves in Fig. 6, *i.e.*,

$$Q_{ox}^{r\text{-}CO_2}(E_r, t_r) = \left(1 - \frac{Q_{dis}^{s}}{Q_{CO}^{s}}\right) \times \int_0^{t_u} [j(E_r, t_r, t) - j(E_r, t_r = 8\ \text{ms}, t)\,dt \quad (4)$$

The upper limit of integration t_u is 20 ms, since we can see that the two curves in Fig. 6 are superimposed at $t > 5$ ms, *i.e.* $\Delta j = j(E_r, t_r, t) - j(E_r, t_r = 8\ \text{ms}, t) = 0$ for $t > 5$ ms. This result demonstrated also that the oxidation of r-CO_2 is a fast process.

The variation of $Q_{ox}^{r\text{-}CO_2}(E_r, t_r)$ with t_r on a Pt(100)-(1) electrode at $E_r = -0.20$ V is plotted in Fig. 7. The $Q_{ox}^{r\text{-}CO_2}(E_r, t_r)$ is increased very rapidly at short t_r. Following further increase in t_r, the increment rate of $Q_{ox}^{r\text{-}CO_2}(E_r, t_r)$ slows progressively, and there is a tendency to approach a saturation value at very long t_r. The insert to this figure illustrates that a linear relationship between $Q_{ox}^{r\text{-}CO_2}(E_r, t_r)$ and t_r is maintained within a few seconds of t_r, the initial rate (υ_i) can thus be calculated from the slope of the straight line, *i.e.*,

$$\upsilon_i(E_r) = \frac{1}{2F}\left.\frac{dQ_{ox}^{r\text{-}CO_2}(E_r, t_r)}{dt_r}\right|_{t_r \to 0} (\text{mol cm}^{-2}\ \text{s}^{-1}), \quad (5)$$

F being the Faraday constant. The initial rate of CO_2 reduction on the Pt(100)-(1) electrode at -0.20 V has been measured, from Fig. 7, as 2.658×10^{-11} mol cm^{-2} s^{-1}, which is a typical value for a surface process and is close to the order of magnitude of the dissociative adsorption rate of small organic molecules on Pt single crystal electrode surfaces.[39]

3.3.2 Variation of the kinetics of CO_2 reduction on Pt(100) electrodes with different surface structures. The distributions of υ_i with E_r on three Pt(100) electrodes of different surface structure, *i.e.*, Pt(100)-(1), Pt(100)($\gamma = 0.5$) and Pt(100)-(2), are illustrated in Fig. 8. In the potential region between 0.20 and 0.05 V, the υ_i is close to 0.7×10^{-12} mol cm^{-2} s^{-1} on the three electrodes, indicating that the reduction of CO_2 on all the three typical surface structures of Pt(100) is very slow. One may notice a small hump near 0.12 V of amplitude 2.1×10^{-12} mol cm^{-2} s^{-1}, in coincidence with the potential of current peak for hydrogen adsorption on (100) sites distributed on the two-dimensional surface domains (Fig. 1). The υ_i increases with progressive decrease in E_r from 0.05 V, and manifests a maximum near -0.19 V on the three curves. It is interesting to observe that υ_i measured at each E_r on the Pt(100)-(1) electrode always has the largest value among those measured on the three electrodes, and the lowest value is measured on the Pt(100)-(2) electrode. The maximum values of υ_i (υ_i^m) measured on the three electrodes at -0.19 V are respectively 2.71×10^{-11}, 1.87×10^{-11} and 1.18×10^{-11} mol cm^{-2} s^{-1}, yielding a diminishing order of reactivity of the three electrodes for CO_2 reduction as Pt(100)-(1) > Pt(100)-($\gamma = 0.5$) > Pt(100)-(2). The above results may presuppose that the kinetics of CO_2 reduction is fastest on (100) sites distributed on the one-dimensional surface domains, and slowest on the two-dimensional surface domains. Hoshi and coworkers[15,19,20] have reported that the reduction of CO_2 on stepped surfaces of a Pt single crystal electrode is much faster than that on a basal plan of a Pt single crystal, illustrating also that the fast kinetics of CO_2 reduction occurr on a stepped (or defected) surface.

Fig. 9 shows the variation with γ of the υ_i^m measured on Pt(100) electrodes of different structures at -0.19 V. Three regions of γ may be discerned. When $\gamma < 0.7$, υ_i^m increases linearly and quickly with increasing γ, a slope of 23.3 mol cm^{-2} s^{-1} is measured. At $\gamma > 1.25$, another linear variation is observed between γ_i^m and υ, but the slope is much smaller, 0.62 mol cm^{-2} s^{-1}. A transition region of γ appears between 0.7 and 1.25, in which υ_i^m no longer varies linearly with γ. According to the definition of γ, two extreme situations of surface structure of a Pt(100) electrode may be the Pt(100) surfaces

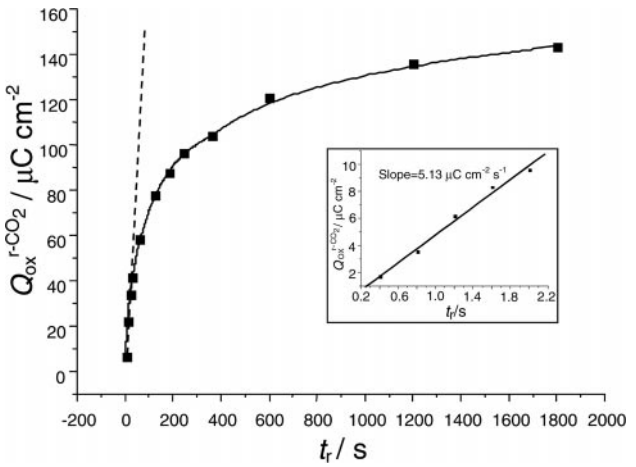

Fig. 7 Illustration of the variation of $Q_{ox}^{r\text{-}CO_2}$ *vs.* t_r for CO_2 reduction at $E_r = -0.2$ V on a Pt(100) electrodes cooled in air after flame annealing. The insert shows the determination of the initial rate of CO_2 reduction.

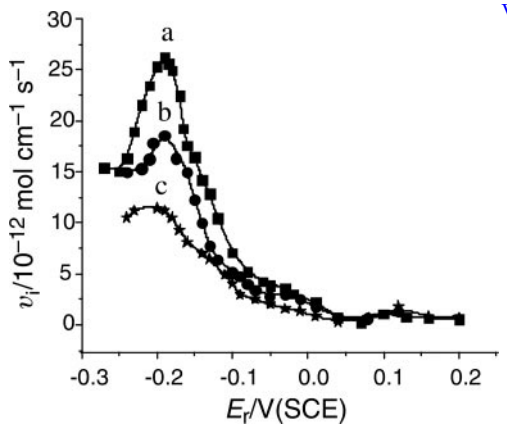

Fig. 8 Distribution of the initial rate of CO_2 reduction on Pt(100) electrodes of different structures, (a) Pt(100)-(1), (b) Pt(100)-($\gamma = 0.5$), and (c) Pt(100)-(2).

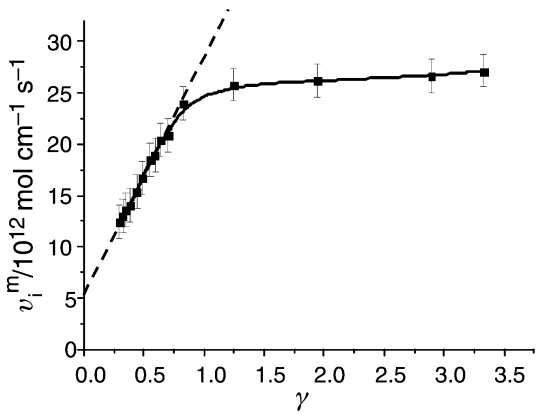

Fig. 9 Variation of the maximum υ_i (υ_i^m) with γ.

with exclusively two-dimensional or one-dimensional surface domains. Such surfaces should yield, respectively, $\gamma = 0$ and $\gamma \to \infty$. We may deduce from Fig. 9 the value of υ_i^m on the Pt(100)-($\gamma = 0$) electrode. By extrapolating the straight line for γ below 0.7 to $\gamma = 0$, the intercept with the υ_i^m axis gives the υ_i^m as 5.3×10^{-12} mol cm^{-2} s^{-1}, which may represent the υ_i^m on a Pt(100) surface with exclusively two-dimensional surface domains, *i.e.*, an ideal surface of Pt(100). This υ_i^m can be considered also as the maximum value of υ_i for CO_2 reduction on (100) sites distributed on the two-dimensional surface domains. It should be pointed out that such an ideal Pt(100) surface could not be obtained under the present conditions, as we may measure from Fig. 2 that γ still equals 0.26, even for a Pt(100) electrode cooled in a H_2-stream after flame annealing. For the same reason, the Pt(100) surface consisting solely of one-dimensional surface domains could not be obtained, since γ is only 3.1 for the Pt(100) electrode cooled in air after flame annealing. A stepped surface of Pt(210) that contains exclusively one-dimensional surface domains of (100) symmetry (or (100) steps) may be a good approximation to an ideal Pt(100) surface with (100) sites all distributed on the one-dimensional surface domains, and is considered to be studied. Although it is impossible to obtain the υ_i^m at $\gamma \to \infty$, we may take simply the value of the υ_i^m measured on the Pt(100)-(1) electrode (*i.e.*, 2.71×10^{-11} mol cm^{-2} s^{-1}) for CO_2 reduction on (100) sites distributed on one-dimensional surface domains, because the slope of the straight line for $\gamma > 1.25$ is very small. It is evident that the reduction of CO_2 on (100) sites distributed on the one-dimensional surface domains is at least 5 times faster than that on (100) sites distributed on the two-dimensional surface domains. The results demonstrated clearly that the Pt(100) surface of short-range order exhibits a higher activity for electrocatalytic reduction of CO_2 than does the Pt(100) surface of long-range order. These results may imply that CO_2 reduction is favored on the step sites or surface defects.

3.4 Further discussion on surface processes involved in CO_2 reduction on Pt(100) electrode

The maximum υ_i, all near -0.19 V in the υ_i–E_r curves of Fig. 8 for CO_2 reduction on Pt(100) electrodes with different surface structures may indicate that hydrogen adatoms (H_{ad}) were involved in the reduction of CO_2, since a high coverage of H_{ad} is certainly achieved at -0.19 V, as illustrated by the cyclic voltammograms in Fig. 1. The CO_2 reduction may thus be thus described as:[4,14]

$$[Pt] + H^+ + e^- \leftrightarrow [Pt]H_{ad} \quad (6)$$

$$CO_2 + [Pt] + [Pt]H_{ad} + H^+ + e^- \rightarrow [Pt]_2CO_{ad} + H_2O \quad (7)$$

or

$$CO_2 + [Pt]H_{ad} + H^+e^- \rightarrow [Pt]CO_{ad} + H_2O \quad (8)$$

where [Pt] denotes a surface site of Pt(100) electrode. The CO_2 may also adsorb on the Pt(100) surface, but this adsorption is very weak[14,40] in comparison with hydrogen adsorption. We have observed from Fig. 4c or in Fig. 5c that the presence of CO_2 in 0.5 M H_2SO_4 solution did not perturb the CV features of hydrogen adsorption, which provides direct evidence for the weak adsorption of CO_2 on the Pt(100) electrode. Three coordination modes of CO_2 adsorption on a transition metal have been proposed in the literature,[1] *i.e.*, side-on coordination (η^2-CO_2), C-coordination (η^1-CO_2) and end-on coordination (η-OCO) shown below,

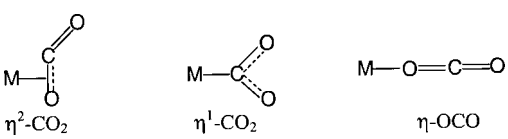

η^2-CO_2 η^1-CO_2 η-OCO

It is know from the above studies that the coverage of r-CO_2 is 0.356 on Pt(100)-(1) and on 0.389 Pt(100)-(2) even though the reduction of CO_2 been carried on at -0.20 V for 2 h, and that the r-CO_2 species adsorb favorably on (100) sites distributed on two-dimensional surface domains. These results may imply that the weakly adsorbed CO_2 species in η^2-CO_2 and η^1-CO_2 adsorption modes can interact easily with hydrogen adatoms adsorbed on adjacent sites to reduce to CO_{ad}. In considering that the υ_i of CO_2 reduction is larger on (100) sites on one-dimensional surface domains than on two-dimensional domains, a migration process of the r-CO_2 species from the one-dimensional surface domains to the two-dimensional surface domains may be involved in reduction of CO on the Pt(100) electrode surface. Ito *et al.*[41,42] have revealed by using *in situ* IR reflection spectroscopy that CO can migrate on Pt single crystal electrode surfaces, which may be additional arguments supporting the above hypothesis concerning the migration of the r-CO_2 species on Pt(100) electrode surface.

5. Conclusions

The present study has concentrated on the surface processes and the kinetics of CO_2 reduction on Pt(100) electrodes with different surface structures. The Pt(100) surface cooled in air after flame annealing (Pt(100)-(1)) is dominated by one-dimensional surface domains and randomly distributed surface defects of short-range order, while that in a H_2-stream (Pt(100)-(2)) contains mainly two-dimensional surface domains of long-range order. Different surface structures of Pt(100) were fabricated by applying a treatment of fast potential cycling (200 V s^{-1}) for different treatment time τ. A parameter γ that is defined as the relative amplitude of current peak for hydrogen adsorption on different surface domains ($j_{P,1}/j_{P,2}$) is used to characterize the surface structure of the Pt(100) electrode. The smaller γ, the more (100) sites are distributed on the two-dimensional surface domains of the Pt(100) electrode.

The *in situ* FTIR spectroscopic studies demonstrated that the products of CO_2 reduction (r-CO_2) on the Pt(100)-(2) are mainly bridge-bonded CO species, but both bridge-bonded CO and linear-bonded CO species were found on the Pt(100)-(1). The small intensity of the IR bands of the r-CO_2 species, even after a long reduction time at -0.20 V, indicated that the maximum coverage of the r-CO_2 that could be reached is rather small. The cyclic voltammetric studies confirmed this point quantitatively, quantitatively and revealed also that the r-CO_2 species adsorbed favorably on (100) sites on two-dimensional surface domains on both the Pt(100)-(1) and Pt(100)-(2) electrodes.

The kinetics of CO_2 reduction on Pt(100) electrodes with different surface structures was investigated by determining quantitatively the initial rate (υ_i) of the reaction, *i.e.* the rate of CO_2 reduction occurring on a clean Pt(100) surface. It was found that the υ_i has an order of magnitude around 10^{-11} mol cm^{-2} s^{-1}. The variation of υ_i with E_r yields a maximum value near -0.19 V on Pt(100) electrodes of different surface structure. The Pt(100)-(1) exhibits a higher υ_i than that of the Pt(100)-(2). Further analysis on the relationship between υ_i^m, *i.e.*, the maximum value of υ_i measured at -0.19 V, and γ led us to conclude that the CO_2 reduction is at least 5 times faster on (100)-sites on one-dimensional surface domains than on (100)-sites on two-dimensional surface domains, illustrating that the CO_2 reduction is favored on step sites and surface defects. Based on the following experimental results: (1) the fast kinetics of CO_2 reduction occurr on Pt(100) surface with predominantly one-dimensional domains (step sites or surface defects); (2) the saturation coverage of the r-CO_2 is rather small; and (3) the r-CO_2 species occupy preferentially surface sites distributed on two-dimensional domains, a process of migration of the r-CO_2 from one-dimensional surface domains

to two-dimensional surface domains is proposed to be involved in CO_2 reduction on a Pt(100) electrode.

The present paper revealed, with quantitative kinetics results and at a microscopic point of view, the surface processes of the electrocatalytic reduction of CO_2 on Pt(100) electrodes. The results demonstrated that the electrocatalytic properties of a Pt single crystal electrode depend strongly not only on the symmetry of the surface sites, but also on the dimension of the surface domains. The new findings advanced the knowledge on electrocatalytic reduction of CO_2, and the fundamentals of electrocatalysis.

Acknowledgement

This study was supported financially through grants of the National Natural Science Foundation of China (NNSFC) and the Education Ministry of China.

References

1 *Electrochemical and Electrocatalytic Reactions of Carbon Dioxide*, ed. B. P. Sullivan, K. Krist and H. E. Guard, Elsevier, Amsterdam, 1993, pp. 19–67 and 145–216.
2 J. Desilvestro and S. Pons, *J. Electroanal. Chem.*, 1989, **267**, 207.
3 B. Z. Nikolic, H. Huang, D. Gervasio, A. Lin, C. Fierro, R. R. Adzic and E. B. Yeager, *J. Electroanal. Chem.*, 1990, **295**, 415.
4 M. L. Marcos, J. Gonzalez-Velasco, J. M. Vara, M. C. Giodano and A. J. Arvia, *J. Electroanal. Chem.*, 1990, **281**, 257.
5 K. Ohkawa, K. Hashimoto and A. Fujishima, *J. Electroanal. Chem.*, 1993, **345**, 445.
6 S. Taguchi, T. Ohmori, A. Aramata and M. Enyo, *J. Electroanal. Chem.*, 1994, **369**, 199.
7 Y. Hori, H. Wakebe, T. Tsukamoto and O. Koga, *Electrochim. Acta*, 1994, **39**, 1833.
8 Y. Hori, H. Wakebe, T. Tsukamoto and O. Koga, *Surf. Sci.*, 1995, **335**, 258.
9 N. Hoshi, T. Uchida, T. Mizumura and Y. Hori, *J. Electroanal. Chem.*, 1995, **381**, 261.
10 N. Hoshi, H. Ito, T. Suzuki and Y. Hori, *J. Electroanal. Chem.*, 1995, **395**, 309.
11 K. Hara, A. Tsuneto, A. Kudo and T. Sakata, *J. Electroanal. Chem.*, 1997, **434**, 239.
12 B. Beden, A. Bewick, M. Razaq and J. Weber, *J. Electroanal. Chem.*, 1982, **139**, 203.
13 J. Sobkowski and A. Czerwinski, *J. Electroanal. Chem.*, 1975, **65**, 327.
14 S. Taguchi and A. Aramata, *Electrochim. Acta*, 1994, **39**, 2533.
15 N. Hoshi, T. Suzuri and Y. Hori, *J. Phys. Chem. B*, 1997, **101**, 8520.
16 A. Rodes, E. Pastor and T. Iwasita, *J. Electroanal. Chem.*, 1994, **369**, 183.
17 A. Rodes, E. Pastor and T. Iwasita, *J. Electroanal. Chem.*, 1994, **373**, 167.
18 A. Rodes, E. Pastor and T. Iwasita, *J. Electroanal. Chem.*, 1994, **377**, 215.
19 N. Hoshi, T. Suzuki and Y. Hori, *J. Electroanal. Chem.*, 1996, **416**, 61.
20 N. Hoshi, T. Suzki and Y. Hori, *Electrochim. Acta*, 1996, **41**, 1647.
21 S.-G. Sun, A.-C. Chen, T.-S. Huang, J.-B. Li and Z.-W. Tian, *J. Electroanal. Chem.*, 1992, **340**, 213.
22 J. Clavilier, *J. Electroanal. Chem.*, 1980, **107**, 205.
23 S.-G. Sun, Y. Lin, N.-H. Li and J.-Q. Mu, *J. Electroanal. Chem.*, 1994, **370**, 273.
24 S.-G. Sun, D.-F. Yang and Z.-W. Tian, *J. Electroanal. Chem.*, 1990, **289**, 177.
25 J. Clavilier and D. Armand, *J. Electroanal. Chem.*, 1986, **199**, 187.
26 D. Armand and J. Clavilier, *J. Electroanal. Chem.*, 1987, **225**, 205.
27 J. Clavilier, J. M. Feliu, A. Fernandez-Vega and A. Aldaz, *J. Electroanal. Chem.*, 1989, **269**, 175.
28 J. Clavilier, K. El Achi, M. Petit, A. Rodes and Am. A. Zamakhchari, *J. Electroanal. Chem.*, 1990, **295**, 333.
29 R. Rodes, M. A. Zamakhchari, K. El Achi and J. Clavilier, *J. Electroanal. Chem.*, 1991, **305**, 115.
30 L. A. Kibler, A. Cuesta, M. Kleinert and D. M. Kolb, *J. Electroanal. Chem.*, 2000, **484**, 73.
31 B. Beden, A. Bewick, K. Kunimatsu and C. Lamy, *J. Electroanal. Chem.*, 1982, **142**, 345.
32 E. Morallon, A. Rodes, J. L. Vazquez and J. M. Perez, *J. Electroanal. Chem.*, 1995, **391**, 149.
33 F. Kitamura, M. Takahashi and M. Ito, *J. Phys. Chem.*, 1988, **92**, 3320.
34 C. S. Kim, C. Korzeniewski and W. J. Tornquist, *J. Chem. Phys.*, 1994, **100**(1), 626.
35 C. S. Kim, W. J. Tornquist and C. Korzeniewski, *J. Phys. Chem.*, 1993, **97**, 6484.
36 B. Beden, C. Lamy, A. Bewick and K. Kunimatsu, *J. Electroanal. Chem.*, 1981, **121**, 343.
37 R. Gomez, J. M. Feliu, A. Aldaz and M. J. Weaver, *Surf. Sci.*, 1998, **410**, 48.
38 J. Clavilier, R. Albalat, R. Gomez, J. M. Orts, J. M. Feliu and A. Aldaz, *J. Electroanal. Chem.*, 1992, **330**, 489.
39 S.-G. Sun, in *Electrocatalysis*, ed. J. Lipkowski and P. Ross, Wiley-VCH, New York, 1998, ch. 6, pp. 253–260.
40 S.-J. Hong, MSc Thesis, Xiamen University, 1998.
41 M. Nakamura, H. Ogasawara, J. Inukai and M. Ito, *Surf. Sci.*, 1993, **283**, 248.
42 S. Watanabe, J. Inkukai and M. Ito, *Surf. Sci.*, 1993, **293**, 1.